Article

Tungsten Oxide-Mediated Photocatalytic Silver Enhancement in a QCM Immunosensor for Alpha-Fetoprotein Detection

Han Sol Kim , Yu Gyeong Cho , Soo Suk Lee *

Posted Date: 16 September 2025

doi: 10.20944/preprints202509.1375.v1

Keywords: alpha-fetoprotein (AFP); sandwich immunoassay; quartz crystal microbalance (QCM) biosensor; tungsten oxide; photocatalytic silver enhancement

 doi:10.20944/preprints202509.1375.v1

Article

Tungsten Oxide-Mediated Photocatalytic Silver Enhancement in a QCM Immunosensor for Alpha-Fetoprotein Detection

Han Sol Kim, Yu Gyeong Cho and Soo Suk Lee *

Department of Pharmaceutical Engineering, Soonchunhyang University, Asan 31538, Republic of Korea

* Correspondence: sslee0810@sch.ac.kr; Tel.: +82-41-530-1394

Abstract

Accurate and early detection of alpha-fetoprotein (AFP) in human serum is essential for the diagnosis and monitoring of hepatocellular carcinoma and related diseases. In this study, we present a highly sensitive and reproducible quartz crystal microbalance (QCM) immunosensor for the quantitative detection of AFP. The detection strategy is based on a sandwich-type immunoassay coupled with a signal amplification method utilizing photocatalytic silver deposition on tungsten(IV) oxide (WO_3) nanoparticles. Since QCM detects resonance frequency shifts induced by mass changes on the sensor surface, the silver-enhanced growth of WO_3 nanoparticles enables significant signal amplification, allowing for precise mass-based quantification. Without amplification, the limit of detection (LOD) for AFP using QCM immunosensor was 286 pg/ml, which was significantly improved to 43.7 pg/ml with photocatalytic silver staining. This approach markedly enhances both sensitivity and reproducibility, offering a robust and efficient platform for clinical biomarker detection and early cancer diagnostics.

Keywords: alpha-fetoprotein (AFP); sandwich immunoassay; quartz crystal microbalance (QCM) biosensor; tungsten oxide; photocatalytic silver enhancement

1. Introduction

Cancer biomarkers are molecular indicators that reflect the biological state of tumors, offering valuable insight into cancer development, progression, and therapeutic responsiveness [1]. In clinical oncology, biomarkers are essential tools for stratifying patients, predicting disease prognosis, and guiding personalized treatment strategies. The sensitivity and specificity of cancer biomarker detection can greatly influence the efficacy of diagnostic and therapeutic decisions [2]. Detection of cancer biomarkers enables early diagnosis, which significantly improves patient prognosis and survival rates. The sensitivity and specificity of cancer biomarker detection can have a significant impact on the efficacy of diagnostic and therapeutic decisions. Despite remarkable advances in cancer treatment, the lack of early and accurate detection methods remains a major challenge, highlighting the need for sensitive biomarker detection platforms [3].

Alpha-fetoprotein (AFP), a glycoprotein produced primarily in the fetal liver and yolk sac, is one of the most widely used biomarkers for hepatocellular carcinoma (HCC) and germ cell tumors (GCTs). Although elevated levels of AFP are associated with malignancies, their presence in small quantities in adult serum necessitates highly sensitive and selective detection methods for clinical application [4,5]. Conventional immunoassays, such as enzyme-linked immunosorbent assays (ELISAs), though widely used, often lack the sensitivity required for early-stage cancer detection or for samples with low AFP concentrations. Therefore, biosensing platforms with enhanced sensitivity and signal amplification capabilities are of growing importance [6–8].

Quartz crystal microbalance (QCM) biosensors have attracted significant attention as mass-sensitive transducers capable of label-free detection of biomolecular interactions. QCM sensors

 doi:10.20944/preprints202509.1375.v1

operate based on the piezoelectric properties of quartz crystals, where the resonance frequency shifts in response to changes in mass on the crystal surface, as described by the Sauerbrey equation. As QCM is capable of detecting real-time mass changes at the sub-nanogram level, it has found broad applications in immunosensing, DNA hybridization, and molecular interaction studies. However, the limited sensitivity of QCM, most notably at low analyte concentrations, has led to the widespread adoption of signal amplification approaches [9–12].

Recent advances in nanotechnology have opened new possibilities for improving biosensor performance. Among these, nanoparticle-mediated signal amplification has shown remarkable potential. Gold nanoparticles (AuNPs) have been widely employed to enhance the QCM signal by increasing the mass on the sensor surface through sandwich-type immunoassay configurations [13–17]. Furthermore, enhancement techniques such as gold staining have enabled even greater signal magnitudes by catalytically growing metal layers around nanoparticle cores. Building on this foundation, alternative approaches utilizing photocatalytic deposition of metals such as silver on nanoparticle surfaces are being investigated for greater signal amplification and cost-effectiveness.

In particular, tungsten(IV) oxide (WO_3) nanoparticles have emerged as a promising photocatalytic material due to their tunable bandgap, chemical stability, and strong oxidative power under UV or visible light. When irradiated, WO_3 generates electron-hole pairs capable of driving redox reactions, such as the reduction of metal ions (e.g., Ag^+) into metallic deposits on the nanoparticle surface [18–21]. This photocatalytic property can be harnessed to amplify the detectable mass on QCM biosensors. By functionalizing WO_3 nanoparticles with antibodies and exposing them to silver ions under UV light, a silver shell can be deposited onto the WO_3 particles, resulting in a significant increase in overall mass and corresponding frequency shift in QCM measurements. Although silver has a lower atomic density and mass than gold, which may result in a relatively smaller signal amplification effect, its photo-induced deposition eliminates the need for additional reducing agents, enabling a more controlled and environmentally benign process [22,23]. Importantly, WO_3 nanoparticles offer a dual functionality, acting both as photocatalysts and as nanocarriers for antibody immobilization, thereby streamlining sensor design and enhancing overall assay performance.

In this study, we report a novel QCM immunosensor for AFP detection that integrates photocatalytic signal amplification via silver deposition on WO_3 nanoparticles. The biosensor is constructed by covalently attaching anti-AFP capture antibodies onto a 3-Glycidyloxypropyltrimethoxysilane (3-GPTMS)-functionalized surface, which promotes stable and efficient antibody binding. A sandwich-type immunoassay is then conducted using AFP-containing serum and detection antibodies conjugated to WO_3 nanoparticles. Upon UV irradiation in the presence of Ag^+, photocatalytic silver deposition occurs selectively on the nanoparticle surface, resulting in a marked increase in resonator mass and corresponding resonance frequency shift. This photocatalytic amplification method represents a significant advancement in QCM biosensing, offering improved sensitivity and lowering detection limits for AFP. Our approach not only broadens the scope of nanoparticle-based signal enhancement strategies but also demonstrates the potential of integrating semiconductor photocatalysts into label-free biosensing platforms. Ultimately, this technology could be extended to other clinically relevant biomarkers, paving the way for broader applications in early disease diagnostics and point-of-care testing.

2. Materials and Methods

2.1. Reagent and Materials

Recombinant Human AFP (ab114216) and two anti-AFP monoclonal antibodies (ab242532 for capture, ab242780 for detector) were purchased from Abcam (Cambridge, UK). AFP-free serum (P61000) was also obtained from BioPacific (Emeryville, CA, USA). Tungsten(IV) oxide (WO_3) nanopowder (< 100 nm particle size) and silver nitrate ($AgNO_3$) for photocatalytic silver deposition, 3-Glycidyloxypropyltrimethoxysilane (3-GPTMS) for surface modification were purchased from

 doi:10.20944/preprints202509.1375.v1

Sigma-Aldrich Chemical Co. (St. Louis, MO, USA) and used without further purification. Bovine serum albumin (BSA) and 10X phosphate-buffered saline (PBS, pH 7.4) was also purchased from Sigma-Aldrich Chemical Co. A 1X PBS solution was prepared by diluting 10X PBS with double-distilled water. All organic solvents were purchased from Samchun Chemical Co., Ltd. (Seoul, South Korea). All aqueous solutions were prepared in double-distilled water from a Milli-Q water-purifying system (18 MΩ cm).

2.2. Design and Configuration of the QCM Measurement System

The QCM measurement system consisted of fluidic and detection modules designed to provide real-time sensor data during assays. Mass changes on silicon dioxide-coated QCM resonators (5 mm diameter; 9 MHz resonance frequency) were monitored by tracking shifts in the resonance frequency of bulk acoustic waves using a QCM922A (Princeton Applied Research, SEIKO EG&G, Tokyo, Japan). The flow cell comprised a peristaltic pump (ISM597; ISMATEC, Glattbrugg, Switzerland), a custom-fabricated fluidic block, and a silicone rubber gasket. Precise fluid control is critical for reliable and user-friendly biomolecular detection in liquid environments. To address this, we developed a specialized fluidic module as shown in Figure 1. The top section of the fluidic block included recessed areas for reaction chambers and gaskets to prevent leakage caused by hydrodynamic pressure, along with integrated fluidic connectors enabling flow across the QCM sensors. Sample and buffer solutions were delivered to the reaction chambers via the peristaltic pump at a constant flow rate of 1.0 mL/min. Each reaction chamber had a volume of 20 μL. After each experiment, the chambers and gaskets were thoroughly rinsed with deionized water followed by 0.05% Tween 20 (Sigma-Aldrich, MO, USA) in PBS. Teflon® tubing (0.032 in. I.D.; The Lee Company, CT, USA) was used to interconnect the fluidic and detection components.

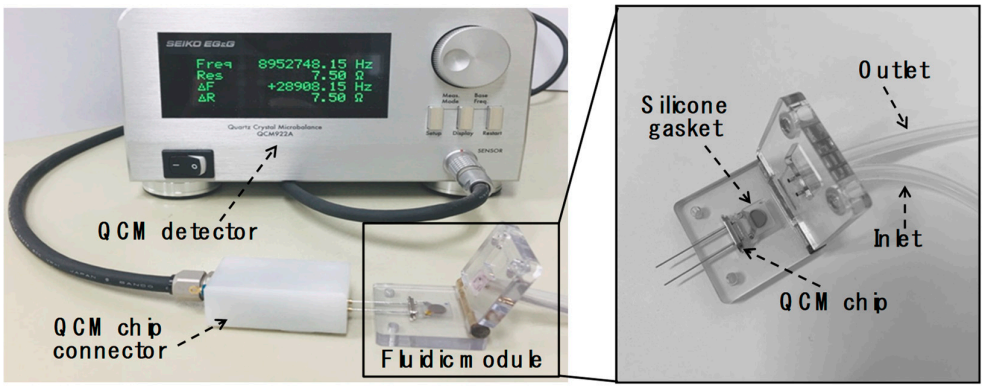

Figure 1. Schematic illustration of the QCM sensor integrated with custom-designed microfluidic modules.

2.3. X-Ray Diffraction (XRD) Analysis

Samples for XRD analysis were prepared by repeated centrifugation and decantation of WO_3 (1.5×10^{-3} M) and Ag-doped WO_3 nanoparticles, both synthesized via photocatalytic silver staining in double-distilled water. The collected residues were oven-dried and analyzed using a Rigaku Miniflex 600 diffractometer (Wilmington, MA, USA). The XRD spectra were recorded in 2-thetha range between 5° and 90°. For TEM imaging, highly diluted suspensions of WO_3 nanoparticles (1.0×10^{-5} M) and WO_3/Ag hybrid nanostructures were prepared in double-distilled water. These samples were sonicated for 2 hours in an ultrasonic bath (Branson Ultrasonics Corp., Danbury, CT, USA) prior to imaging.

2.4. UV–Vis Spectroscopic Analysis of Silver-Doped WO_3 Nanostructures

To evaluate the photocatalytic activity of WO_3 nanoparticles in the reduction of silver ions, the nanoparticles were dispersed in aqueous $AgNO_3$ solutions with concentrations ranging from 0 to 20

 doi:10.20944/preprints202509.1375.v1

mM. The mixtures were subjected to UV irradiation at a wavelength of 365 nm for durations ranging from 0 to 20 min using a handheld UV lamp. Upon irradiation, the solutions progressively developed a dark gray coloration, indicative of the formation of silver nanoparticles via photocatalytic reduction. The extent of silver nanoparticle generation was quantitatively assessed using UV–visible absorption spectroscopy. Absorbance measurements were performed in 96-well microplates (Thermo Fisher Scientific, Bremen, Germany) using an Epoch 2 microplate spectrophotometer (BioTek Instruments, Winooski, VT, USA). Each experimental condition was tested in quintuplicate to ensure reproducibility and statistical reliability.

2.5. Preparation of Antibody-Conjugated WO_3 Nanoparticles for AFP Biosensing

WO_3 nanoparticles (average diameter ~21 nm) were initially purified by sequential washing with methanol and deionized water, followed by drying in an oven at 80 °C. Surface activation was achieved by immersing the nanoparticles in 10 mL of freshly prepared piranha solution (H_2SO_4/H_2O_2 = 3:1, v/v) for 10 min. After thorough rinsing with deionized water, the activated nanoparticles were functionalized by treatment with 5% (v/v) 3-glycidyloxypropyltrimethoxy-silane (3-GPTMS) in methanol for 1 h at room temperature. The GPTMS-treated nanoparticles were subsequently washed with methanol (2 min), dried under a nitrogen (N_2) stream, and cured at 110 °C for 1 h in a dry oven. Post-curing, the particles were again washed with methanol and dried under N_2 to remove any unbound silane. For antibody conjugation, 10 μL of anti-AFP detecting antibody (1 mg/mL) was added to 1 mL of the GPTMS-modified WO_3 nanoparticle suspension. The mixture was gently agitated at room temperature for 1 h to facilitate covalent binding. To block residual active sites and minimize nonspecific binding, 0.1 mL of 1% bovine serum albumin (BSA) in 1× phosphate-buffered saline (PBS, pH 7.4) was added, followed by incubation for 30 min at room temperature. The resulting antibody-conjugated WO_3 nanoparticles were collected by centrifugation at 13,000 rpm for 10 min at 4 °C. After discarding the supernatant, the pellet was resuspended in 0.5 mL of 1× PBS containing 0.1% BSA and stored for subsequent use.

2.6. WO_3-Mediated Photocatalytic Silver Staining in Sandwich Immunoassay for AFP Detection

The SiO_2-coated QCM sensor surface was first cleaned by sequential rinsing with deionized water and absolute ethanol, followed by nitrogen (N_2) drying. The cleaned chip was then subjected to surface activation using UV/ozone treatment for 10 min. Subsequently, the activated surface was functionalized by immersion in 5% (v/v) 3-glycidyloxypropyl-trimethoxysilane (3-GPTMS) in methanol for 1 h at room temperature. Afterward, the chip was rinsed with methanol (2 min), dried under N_2, and cured at 110 °C for 1 h. A final methanol rinse and N_2 drying completed the silanization process. To immobilize the capture antibodies, 30 μL of anti-AFP antibody solution (100 μg/mL in PBS, pH 7.4) was deposited onto the GPTMS-modified QCM surface and incubated for 1 h in a humidity chamber to prevent evaporation. Unreacted surface sites were subsequently blocked with 3% bovine serum albumin (BSA) in PBS (pH 7.4) to minimize nonspecific binding during subsequent assay steps. Following surface preparation, 50 μL aliquots of AFP-spiked AFP-free human serum at various concentrations were applied to the sensor and incubated for 30 min to allow antigen binding. The surface was then washed with PBS (1 min), and 50 μL of WO_3 nanoparticle-conjugated anti-AFP detecting antibody was introduced. After a further 30 min incubation, the chip was again washed with PBS (1 min). For signal amplification, 5 mM $AgNO_3$ solution was added, and the sensor surface was irradiated with UV light (365 nm) using a 4 W handheld UV lamp (Vilber Lourmat, France) for 10 min to initiate photocatalytic silver deposition mediated by the WO_3 nanoparticles. The sensor was finally washed with PBS to remove excess reagents. All measurements were performed in triplicate for each AFP concentration, with independent replicates conducted on different days to ensure reproducibility. In addition, a blind test was conducted using five serum samples spiked with unknown concentrations of AFP. Each 1 mL sample was analyzed using both the developed QCM sensor platform and the commercial VIDAS® immunoassay system (BioMérieux, Marcy L'Étoile, France) to assess comparative performance.

 doi:10.20944/preprints202509.1375.v1

3. Results and Discussion

3.1. Strategies for Sensitive AFP Immunoassay: Detection and Signal Amplification Approaches

Scheme 1 presents the overall strategy for AFP detection, which is based on a conventional sandwich immunoassay format coupled with a photocatalytic signal amplification mechanism. In this approach, anti-AFP capture antibodies were covalently immobilized onto a QCM sensor surface pre-functionalized with 3-glycidyloxypropyltrimethoxysilane (3-GPTMS). Upon exposure to serum containing AFP, the target proteins specifically bound to the immobilized antibodies, forming the primary immune complex. Subsequently, detection antibodies conjugated to WO_3 nanoparticles were introduced to form a complete sandwich structure. To amplify the sensor signal, the bound WO_3 nanoparticles underwent a photocatalytic silver staining reaction, which increased their size and mass, thereby enhancing the resonance frequency shift measured by the QCM. This signal amplification was achieved through UV-induced reduction of silver ions (Ag^+) on the WO_3 nanoparticle surface, resulting in the formation of a WO_3/Ag composite. The silver deposition step was critical for achieving sufficient signal intensity, as the resonance frequency shift without this amplification was negligible and inadequate for reliable AFP quantification. These results indicate that the majority of the observed frequency change during AFP detection originated from the photocatalytic silver staining process.

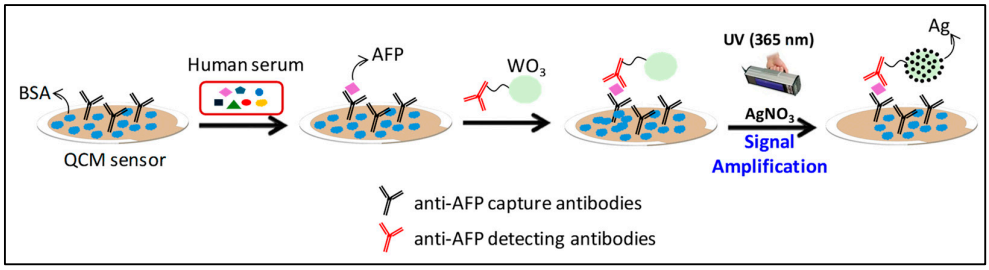

Scheme 1. Schematic representation of the QCM-based AFP sandwich immunoassay integrated with WO_3-mediated photocatalytic silver enhancement for signal amplification.

To confirm the successful formation of the WO_3/Ag composite, X-ray diffraction (XRD) analysis was conducted to investigate the crystal structures of WO_3 and Ag-doped WO_3 nanostructures, as well as to confirm the presence of silver particles on the WO_3 surface following photocatalytic silver deposition. For comparison, the XRD pattern of pristine WO_3 was also recorded. The diffraction results for both WO_3 and Ag/WO_3 specimens are presented in Figure 2. As shown in Figure 2, the typical diffraction spectrum of WO_3 crystals exhibits the characteristic peaks of tungsten oxide. The XRD patterns of Ag-loaded WO_3 clearly display the same set of peaks observed for pure WO_3, confirming the incorporation of silver into the tungsten oxide lattice. A distinct peak appearing at approximately 38.6° was identified as the (111) main reflection of metallic silver, which was absent in the pristine WO_3 sample. These XRD results validate the successful fabrication of Ag/WO_3 nanostructures through photocatalytic deposition of silver.

 doi:10.20944/preprints202509.1375.v1

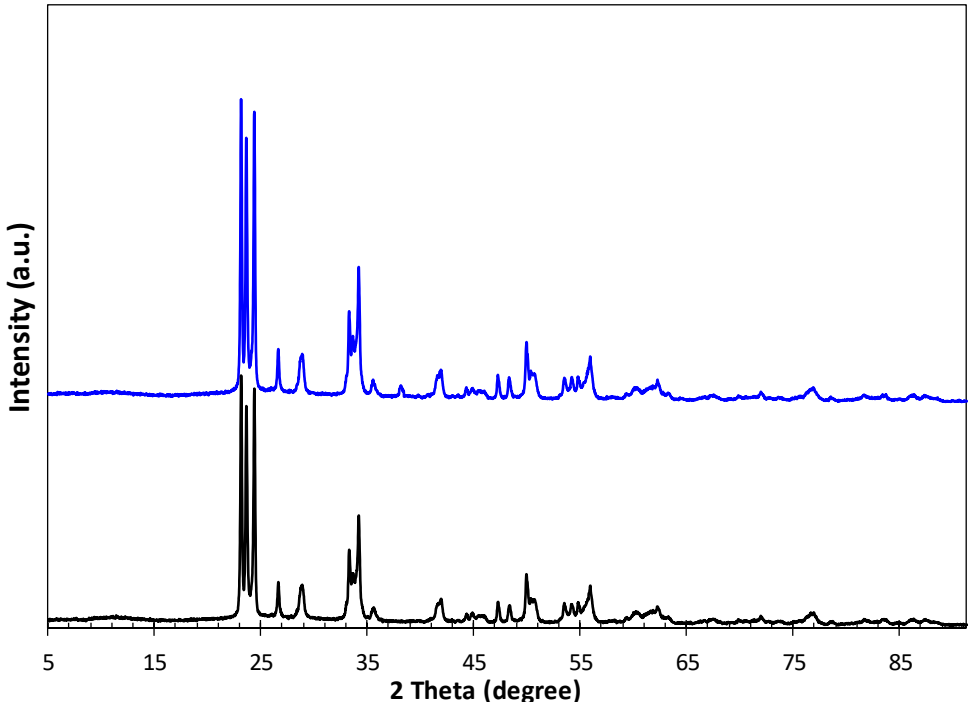

Figure 2. XRD profiles of WO_3 and Ag/WO_3, highlighting changes in crystalline structure upon silver incorporation.

3.2. Signal Amplification Process: WO_3-Based Photocatalytic Silver Staining

To improve the detection sensitivity of the QCM-based sandwich immunoassay, we performed a photocatalytic silver staining reaction, which is crucial for amplifying the mass-induced resonance shift of the QCM sensor. Given that the silver staining process relies on UV-induced reduction of Ag^+ ions in aqueous $AgNO_3$ solution in the presence of WO_3 nanoparticles, two critical factors were investigated: $AgNO_3$ concentration and UV irradiation time. Throughout this process, the intensity of UV light was held constant to exclude its influence on reaction kinetics. First, the effect of UV irradiation duration was assessed by dispersing WO_3 nanoparticles in 10 mM $AgNO_3$ solution and monitoring the absorption band appeared in the visible region, which is a typical phenomenon associated with silver formation [24]. As shown in Figure 3(a), the UV–vis spectra recorded at various time points revealed a progressive increase in absorbance at 400 nm with prolonged UV exposure. Based on the rate of absorbance increase and the overall immunoassay time for AFP detection, we determined that 5 minutes of UV irradiation was sufficient. Next, the influence of $AgNO_3$ concentration was investigated under the fixed condition of 10 minutes UV exposure. As shown in Figure 3(b), the absorbance at 400 nm increased with increasing $AgNO_3$ concentration up to 20 mM. A concentration of 10 mM was considered sufficient to achieve uniform and stable silver deposition. At higher concentrations, excessive nucleation of silver could lead to uncontrolled nanoparticle growth and potential detachment from the WO_3 surface. This was further evidenced in QCM experiments, where sensor instability and signal deterioration were observed due to silver nanoparticle aggregation and shedding from the surface. Based on these observations, the conditions for WO_3-mediated photocatalytic silver staining were established as 10 mM $AgNO_3$ and 5 minutes of UV irradiation. These parameters were employed in all subsequent signal amplification steps within the AFP sandwich immunoassay.

 doi:10.20944/preprints202509.1375.v1

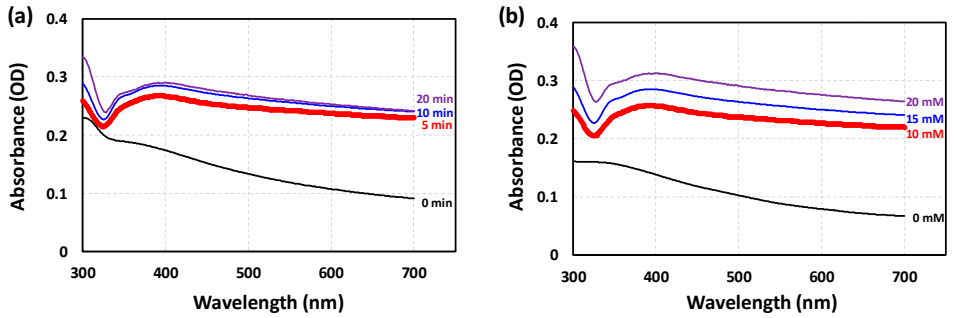

Figure 3. UV–VIS absorption spectra of WO_3 nanoparticles: (a) dispersed in 10 mM $AgNO_3$ solution under different UV irradiation times (0, 5, 10, and 20 min), and (b) suspensions after 5 min of UV irradiation in $AgNO_3$ solutions with varying concentrations (0, 10, 15, and 20 mM).

3.3. Real-Time QCM Sensor Response for AFP Detection

Figure 4 illustrates the real-time changes in resonance frequency and resistance of the QCM sensor during the stepwise detection of AFP. The sensing process comprises three main stages: (1) immobilization and binding of AFP to surface-anchored capture antibodies, (2) formation of sandwich complexes through the introduction of WO_3-conjugated detection antibodies, and (3) signal amplification via photocatalytic silver staining, leading to size enhancement of the WO_3 nanoparticles. The entire process takes approximately 30 min. As anticipated, the resonance frequency decreased progressively due to mass accumulation on the sensor surface during each sequential step, while the resonance resistance concurrently increased, reflecting energy dissipation associated with the growing viscoelastic layer [25]. The blue bold line in Figure 4 represents the temporal decrease in resonance frequency observed during AFP detection at a concentration of 10 ng/mL. Notably, the most significant shifts in both parameters occurred during the photocatalytic silver deposition phase. This amplification step, in which metallic silver was selectively deposited onto the surface of WO_3 nanoparticles, substantially increased the total mass bound to the sensor, resulting in a pronounced frequency drop. These findings underscore the critical role of the silver staining step in enhancing signal magnitude. In the absence of this step, the sensor exhibits a markedly weaker response, thereby compromising detection sensitivity. Thus, the incorporation of photocatalytic silver amplification is essential for achieving ultrasensitive AFP detection using the QCM platform. The substantial increase in mass observed on the QCM sensor surface following the photocatalytic deposition of metallic silver onto WO_3 nanoparticles resulted in a pronounced decrease in resonance frequency, as described by the Sauerbrey equation (Equation (1)) [26]:

$$\Delta f = -[2f_0^2 / A(\rho_q \mu_q)^{1/2}]\Delta m \quad (1)$$

where f_0 is the fundamental resonance frequency (8.953×10^6 Hz), Δf is the change in frequency (Hz), Δm is the change in mass (g), A is the active area of the piezoelectric quartz crystal (0.196 cm^2), and ϱ_q and μ_q represent the mass density (2.648 g/cm^3) and shear modulus (2.947×10^{11} $g \cdot cm^{-1} \cdot s^{-2}$) of AT-cut quartz, respectively.

 doi:10.20944/preprints202509.1375.v1

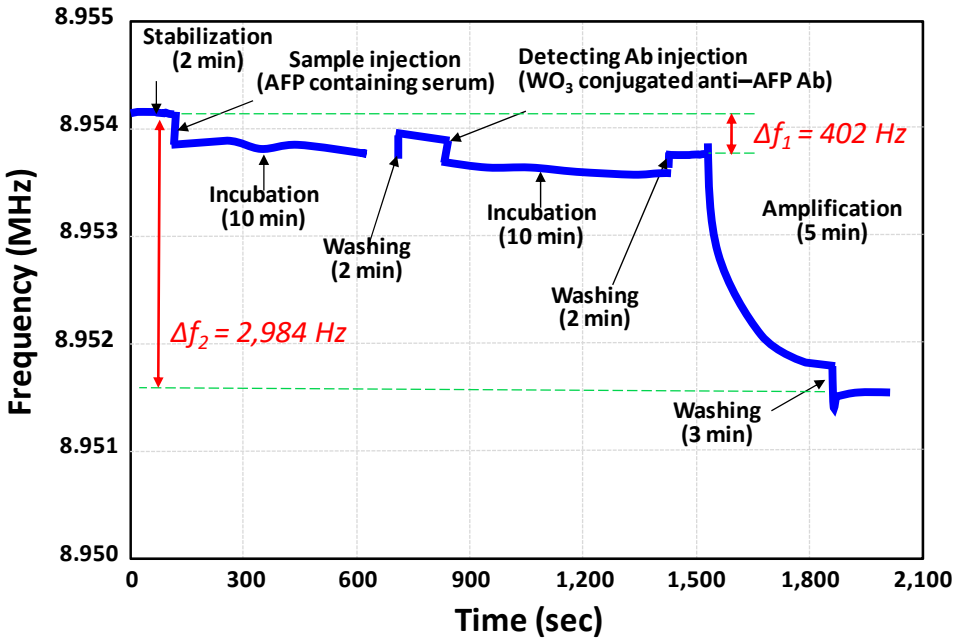

Figure 4. Real-time QCM sensor response to 10 ng/mL of AFP in human serum, detected via WO_3-conjugated antibody sandwich immunoassay followed by photocatalytic silver staining for signal amplification. The observed decrease in resonance frequency corresponds to the increase in effective mass on the QCM sensor surface. The total frequency shift (Δ frequency) is indicated by the red double-headed arrow in the figure. Δf_1 and Δf_2 represent the frequency changes induced by the sandwich immunoassay alone and the subsequent photocatalytic silver deposition, respectively.

3.4. Improving AFP Detection Sensitivity Using WO_3-Mediated Photocatalytic Silver Staining

We investigated the effect of varying concentrations of alpha-fetoprotein (AFP) ranging from 50 pg/mL to 100 ng/mL in troponin-free human serum on the resonance frequency shifts of a QCM sensor during a sandwich immunoassay followed by photocatalytic silver staining. For each AFP concentration, the average frequency shift was calculated from three independent experiments. As depicted in Figure 5, the resonance frequency shift increased logarithmically with increasing AFP concentration. At higher AFP concentrations, a greater amount of the target protein was captured by the immobilized paired antibodies, resulting in an increased accumulation of WO_3 nanoparticles conjugated to the detection antibody on the QCM sensor surface. This increase in surface-bound nanoparticles contributed to the mass loading on the sensor and was further amplified by the enlargement of the WO_3 nanoparticles via the photocatalytic silver deposition process. To isolate the mass-loading effect from other confounding factors, frequency shifts at each concentration were corrected by subtracting the blank values. This correction was essential to eliminate the influence of non-specific factors such as solution viscosity and temperature fluctuations, which were introduced during the silver staining process involving the addition of $AgNO_3$ and UV irradiation. It is well known that in most QCM-based biomolecular detection systems, the thickness of the adsorbed biomolecular layer is typically much smaller than the viscous penetration depth in the liquid phase. Therefore, viscosity changes can significantly affect the resonance frequency. However, in this study, the presence of a signal amplification step involving photocatalytic nanoparticle growth necessitated rigorous blank subtraction to ensure that the observed frequency changes reflected only the mass-loading effect due to AFP binding.

The blue plot in Figure 5 illustrates the results of a WO_3 nanoparticle-conjugated sandwich immunoassay without signal amplification, while the upper red plot shows the enhanced response achieved through photocatalytic silver staining-mediated signal amplification. As previously

 doi:10.20944/preprints202509.1375.v1

described, the silver staining process significantly contributed to the overall decrease in resonance frequency due to the increased mass loading and nanoparticle growth on the sensor surface. Signal amplification using photocatalytic silver staining (red plot) substantially improved the sensor's sensitivity, achieving a limit of detection (LOD) for AFP of 43.7 pg/mL. In contrast, the LODs for the assays without amplification were 286 pg/mL (blue plot). In all cases, the LOD, calculated according to Shrivastava and Gupta [27], was defined as follows

$$LOD = Mean_{blank} + 1.645(SD_{blank}) + 1.645(SD_{low\ concentration\ sample})$$

Owing to the enhanced signal intensity from silver deposition, the detectable AFP concentration was significantly reduced—representing approximately 6.54-fold improvements in LOD compared to the blue plot. Furthermore, the linear correlation (R^2) between AFP concentration and resonance frequency improved with signal amplification. The correlation coefficient increased from 0.9668 (red plot) to 0.9896 (blue plot) with silver staining (Figure 5), indicating better linearity and quantitative reliability. The coefficient of variation (CV), a key factor for reproducibility, was 30.6% at the lowest AFP concentration (50 pg/mL) for the red plot. However, when the same assay was followed by photocatalytic silver staining, the CV values across all tested concentrations were reduced to below 13.6%, demonstrating significantly improved assay precision (Supplementary material S1). Taken together, these findings indicate that the QCM-based AFP immunosensor employing WO_3 nanoparticle-mediated photocatalytic silver staining provides a highly sensitive and reproducible platform, with an LOD of 43.7 pg/mL. This performance is comparable to, or better than, several recently reported nanomaterial-based AFP biosensors. A comparative summary of LODs from various detection methods, including the present study, is provided in Table 1.

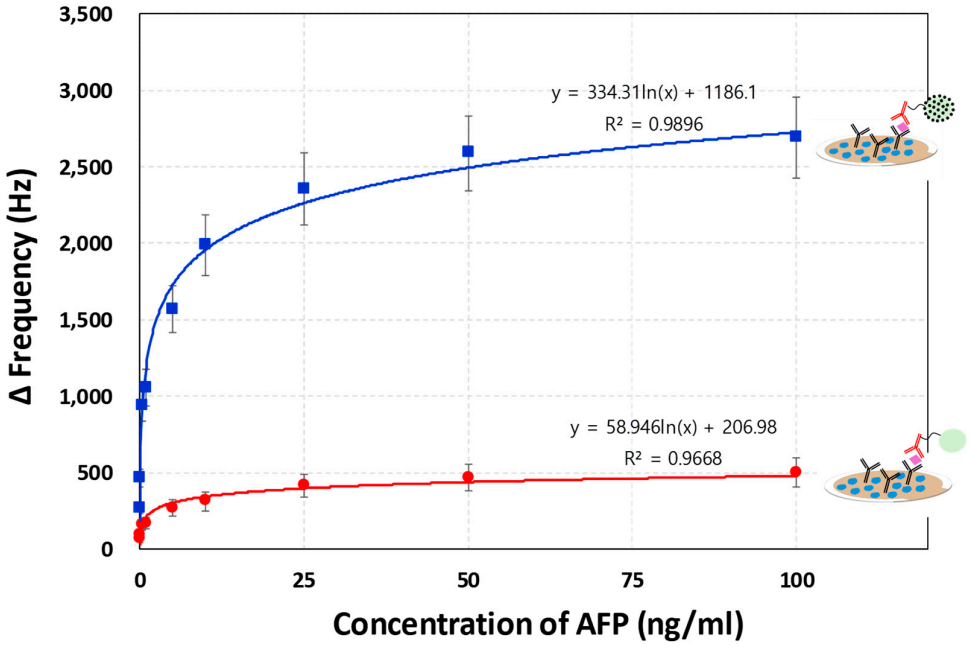

Figure 5. Resonance frequency shifts of the QCM immunosensor at various AFP concentrations (50 pg/mL – 100 ng/mL). The red plot illustrates results from the sandwich immunoassay using WO_3 nanoparticle-conjugated detection antibodies without signal amplification. The blue plot at the top shows the enhanced frequency shifts obtained through photocatalytic silver staining-based signal amplification.

 doi:10.20944/preprints202509.1375.v1

Table 1. Comparison of LODs in nanomaterial-assisted AFP detection with reported methods.

Detection Technique	Nanomaterials	LOD (pg/ml)	Linear Range (ng/ml)	Reference
Colorimetry	AuNP[4]	83	10 – 300	[28]
Colorimetry	ZnS-CdTe	10	0.05 – 12	[29]
Fluorescence	Carbon dots	474	10 – 100	[30]
Fluorescence	AuNP	1.51	0.01 – 0.8	[31]
Chemiluminescence	AuNP-Fe_3O_4	0.067	0.0001 – 1.0	[32]
Electrochemistry	Ag/Bi_2S_3/TiO_2 nanorod	5.1	0.002 – 100	[33]
Electrochemistry	AuNPs–MXene composite	50	1.0 – 300	[34]
SPR[1]	Label-free	5.4	0.5 – 3.0	[35]
SERS[2]	AuNP	500	0.5 – 1,000	[36]
ECL[3]	$Ru(bpy)_3^{2+}$/β-cyclodextrin	0.0011	0.00001 – 50	[37]
QCM	AuNP	56	0.05 – 100	[38]
QCM	WO_3/Ag	43.7	0.05 –100	This work

[1] SPR: Surface plasmon resonance; [2] SERS: Surface Enhanced Raman Spectroscopy; [3] ECL: Electrochemiluminescence; [4] AuNP: Gold nanoparticle.

3.5. Evaluation of QCM Sensor Performance Using Blind-Spiked AFP Samples

To validate the practical utility and analytical accuracy of our QCM-based immunoassay for AFP detection, a blind-spiked sample analysis was conducted using both our QCM sensor platform and a commercial reference system, the VIDAS® immunoassay (bioMérieux, Marcy L'Étoile, France). Seven serum samples were independently prepared by spiking an undisclosed amount of AFP into AFP-free human serum (1 mL each). These blind samples were analyzed using the two systems, and the results were compared. In the QCM system, the resonance frequency shifts measured for the blind samples were converted into AFP concentrations using the standard calibration curve derived from the upper (blue) plot in Figure 5. The AFP concentrations obtained from both the QCM and VIDAS® systems are presented in Supplementary material S2. For the QCM system, the mean value of three replicate measurements was used, while the VIDAS® results represent the average of two replicates. Relative errors were calculated as the percentage difference between the QCM and VIDAS® results, normalized to the VIDAS® values. Although the AFP concentrations measured by the QCM system were slightly lower overall compared to those from the clinically validated VIDAS® system, the relative errors ranged between 20–35 %. Despite these deviations, the two methods showed acceptable agreement across the entire AFP concentration range tested (0.5 ng/mL to 50 ng/mL), as illustrated in Figure 6. Deming regression analysis revealed a strong correlation between the two methods, with a correlation coefficient (R) of 0.9996 and a slope of 0.8287. Considering the methodological and calibration differences between the two systems, the proportional bias indicated by the slope was deemed acceptable [39]. Additionally, the recovery rates of AFP spiked into human serum at three concentrations (5, 10, and 50 ng/mL) were assessed using the QCM immunoassay with photocatalytic silver staining. The observed recovery rates ranged from 116% to 123%, further supporting the quantitative performance of the developed assay (Supplementary material S3).

 doi:10.20944/preprints202509.1375.v1

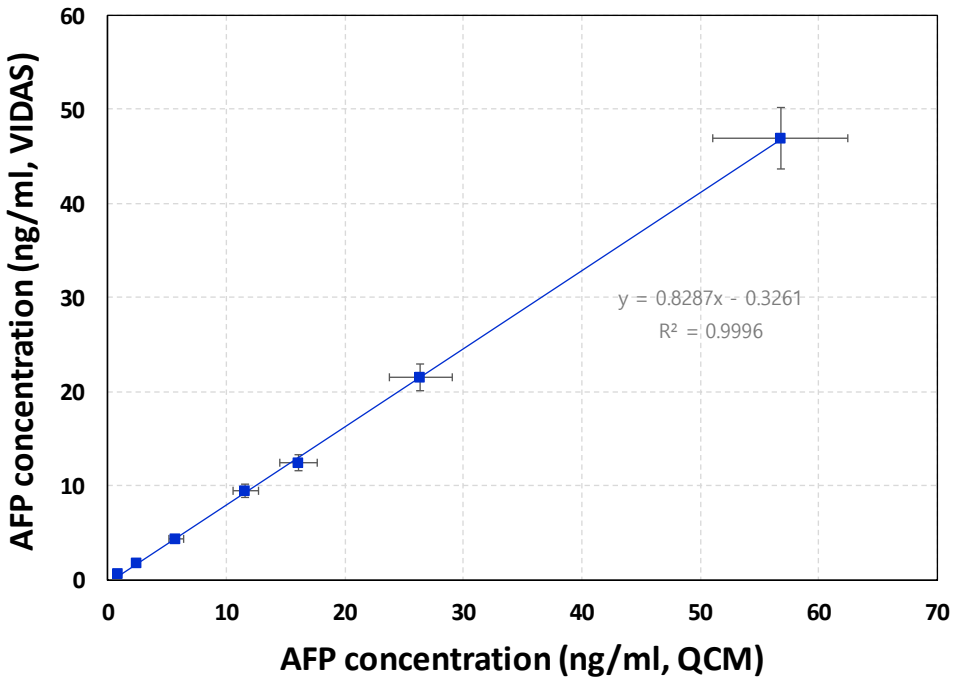

Figure 6. Correlation analysis between AFP concentrations measured by the developed QCM sensor system and the commercial VIDAS® immunoassay for seven blind-spiked human serum samples. A strong agreement was observed between the two methods across the entire tested concentration range (0.5 ng/mL to 50 ng/mL), demonstrating the quantitative reliability of the QCM-based assay.

4. Conclusions

In this study, we successfully developed a sandwich immunoassay combined with a WO_3-mediated photocatalytic silver staining technique for signal amplification, enabling highly sensitive and reproducible detection of AFP in human serum. The substantial enhancement in resonance frequency shift induced by the signal amplification markedly improved both the sensitivity and reproducibility of the assay. Given these advantages, the proposed QCM sensing platform holds great promise for broad applications in immunoassays and biomarker detection. Future work will focus on advancing the QCM biosensor system towards point-of-care testing by integrating automated fluidics and multiplexed target detection. In this context, a cartridge-based device incorporating a QCM sensor chip and a UV irradiation module capable of automated fluid control is envisioned, with materials such as quartz that allow efficient transmission of 365 nm UV light being essential for optimal performance.

Supplementary Materials: The following supporting information can be downloaded at website of this paper posted on Preprints.org, Table S1: QCM signal intensities (changes in resonance frequency) and % CV values; Table S2: Blind-spiked AFP sample tests using our QCM sensing system and the VIDAS® immunoassay system; Table S3: Recovery rate of spiked AFP in human serum tested by our QCM sensing system

Author Contributions: Conceptualization, S.L.; methodology, H.K.; software, H.K.; validation, S.L., H.K.; formal analysis, H.K.; investigation, S.L.; resources, S.L.; data curation, H.K. and Y.C; writing—original draft preparation, S.H.; writing—review and editing, H.K.; visualization, Y.C.; supervision, S.L.; project administration, S.L.; funding acquisition, S.L. All authors have read and agreed to the published version of the manuscript.

Funding: This work was supported by the Basic Science Research Program through the National Research Foundation of Korea (NRF-2022R1F1A1067428).

 doi:10.20944/preprints202509.1375.v1

Institutional Review Board Statement: Not applicable.

Informed Consent Statement: Not applicable.

Data Availability Statement: Data are contained within the article.

Acknowledgments: This work was supported by Soonchunhyang University. This work was also the results of a study on the "Regional Innovation System & Education (RISE)" Project, supported by the Ministry of Education of Korea and Chungnam RISE.

Conflicts of Interest: The authors declare no conflicts of interest.

References

1. Passaro, A.; Bakir, M.A.; Hamilton, E.G.; Diehn, M.; Andre, F.; Roy-Chowdhuri, S.; Mountzios, G.; Wistuba, I.I.; Swanton, C.; Peters, S. Cancer biomarkers: Emerging trends and clinical implications for personalized treatment. Cell **2024**, *187*, 1617-1635.
2. Das, S.; Dey, M.K.; Devireddy, R.; Gartia, M.R. Biomarkers in cancer detection, diagnosis, and prognosis. *Sensors* **2023**, *24*, 37.
3. Mustafa, S.K.; Khan, M.F.; Sagheer, M.; Kumar, D.; Pandey, S. Advancements in biosensors for cancer detection: revolutionizing diagnostics. Med.l Oncol. **2024**, *41*, 73.
4. Kim, H.; Jang, M.; Kim, E.. Exploring the Multifunctional Role of Alpha-Fetoprotein in Cancer Progression: Implications for Targeted Therapy in Hepatocellular Carcinoma and Beyond. *Int. J. Mol. Sci.* **2025**, *26*, 4863.
5. Lu, Y.; Lin, B.; li, M. The role of alpha-fetoprotein in the tumor microenvironment of hepatocellular carcinoma. Front. Oncol. **2024**, *14*, 1363695.
6. Niaki, N.M.; Hatefnia, F.; Heidari, M.M.; Tabean, M.; Mobed, A. Alpha-Fetoprotein (AFP) biosensors. Clin. Chim. Acta **2025**, *573*, 120293.
7. Jia, Y.; Zhao, H.; Huang, S.; Yin, F.; Wang, W.; Hu, Q.; Wang, Y.; Feng, B.. Rapid and portable detection of hepatocellular carcinoma marker alpha-fetoprotein using a droplet evaporation-based biosensor. *Talanta* **2025**, *294*, 128189.
8. Ramachandran, L.; Rub, F.A.; Hajja, A.; Alodhaibi, I.; Arai, M.; Alfuwais, M.; Makhzoum, T.; Yaqinuddin, A.; Al-Kattan, K.; . Assiri, A.M.; Broering, D.C.; Chinnappan, R.; Mir, T.A.; Mani, N.K. Biosensing of Alpha-Fetoprotein: A Key Direction toward the Early Detection and Management of Hepatocellular Carcinoma. *Biosensors* **2024**, *14*, 235.
9. Alanazi, M.; Almutairi, M.; Alodhayb, A.N. A Review of quartz crystal microbalance for chemical and biological sensing applications. Sens Imaging **2023**, *24*, 10.
10. Akgönüllü, S.; Özgür, E.; Denizli, A. Recent Advances in Quartz Crystal Microbalance Biosensors Based on the Molecular Imprinting Technique for Disease-Related Biomarkers. *Chemosensors* **2022**, *10*, 106.
11. Lino, C.; Barrias, S.; Chaves, R.; Adega, F.; Fernandes, J.R.; Martine-Lopes, P. Development of a QCM-based biosensor for the detection of non-small cell lung cancer biomarkers in liquid biopsies. Talanta **2023**, *260*, 124624.
12. Lim, J.Y.; Lee, S.S. Quartz crystal microbalance cardiac Troponin I immunosensors employing signal amplification with TiO_2 nanoparticle photocatalyst. *Talanta* **2021**, *228*, 122233.
13. Safari, Z.; Cohan, R.A.; Sepahi, M.; Sadeqi, M.; Khoobi, M.; Fard, M.H.; Ghavidel, A.; Amiri, F.B.; Aghasadeghi, M.R.; Norouzian, D. Signal amplifcation of a quartz crystal microbalance immunosensor by gold nanoparticles-polyethyleneimine for hepatitis B biomarker detection. Sci. Reports **2023**, *13*, 21851.
14. Pohanka, M. Quartz crystal microbalance biosensor for the detection of procalcitonin. Talanta **2023**, *257*, 124325.
15. Min, H.J.; Mina, H.A.; Deering, A.J.; Robinson, J.P.; Bae, E. Detection of Salmonella Typhimurium with gold nanoparticles using quartz crystal microbalance biosensor. *Sensors* **2022**, *22*, 8928.
16. Lim, J.Y.; Lee, S.S. A QCM immunosensor employing signal amplification strategies by enlarging the size of nanoparticles using gold or silver staining. *Analyst* **2022**, 147, 5725-5731.
17. Kwak, J.; Lee, S.S.. Highly sensitive piezoelectric immunosensors employing signal amplification with gold nanoparticles. *Nanotechnology* **2019**, *30*, 445502.

 doi:10.20944/preprints202509.1375.v1

18. Ghazal, S.; Mirzaee, M.; Darroudi, M.; Sabouri, Z.; Khadempir, S. Chitosan-based synthesis of silver-doped tungsten oxide nanoparticles and assessment of its cytotoxicity and photocatalytic performance. J. Photochem. Photobiol. A Chem. **2024**, *448*, 115323.
19. Loka, C.; Lee, K.-S. Dewetted silver nanoparticle-dispersed WO_3 heterojunction nanostructures on glass fibers for efficient visible-light-active photocatalysis by magnetron sputtering. *ACS Omega* **2022**, *7*, 1483-1493.
20. Matalkeh, M.; Nasrallah, G.; Shurrab, F.M.; Al-Absi, E.S.; Mohammed, W.; Elzatahry, A.; Saoud, L.M. Visible light photocatalytic activity of Ag/WO_3 nanoparticles and its antibacterial activity under ambient light and in the dark. *Results Eng.* **2022**, *13*, 100313.
21. Pourcin, F; Bernardini, S.; Videlot-Ackermann, C.; Nambiema, N.; Liu, J.; Liu, L.; Aguir, K., Margeat, O.; Ackermann. J. Silver Growth on Tungsten Oxide Nanowires for Nitrogen Dioxide Sensing at Low Temperature. *Proceedings* **2018**, *2*, 946.
22. Cao, X.; Tan, B.; Zhang B.; Huang, G.; Xu, H.; Song, Z.; Yan, J. Integration of silver nanoparticles into carbon-encapsulated tungsten oxide promoting visible-light-driven photocatalytic degradation efficiency. Appl. Surf. Sci. **2024**, *678*, 161112.
23. Can, F.; Courtois, X.; Duprez, D. Tungsten-Based Catalysts for Environmental Applications. *Catalysis* **2021**, *11*, 703.
24. Hussain, A.; Fiaz, S.; Almohammedi, A; Waqar, A. Optimizing photocatalytic performance with AG-doped ZNO nanoparticles: Synthesis and characterization. Heliyon, ***2024***,*10, e35725*.
25. Muramatsu, H.; Kawamura, M.; Tanabe, S.; Suda, M. Basic characteristics of quartz crystal sensor with interdigitated electrodes. Anal. Chem. Res. **2016**, *7*, 23-30.
26. Cimmino, W.; Raucci, A.; Grosso, S.P.; Normanno, N.; Cinti, S. Enhancing sensitivity towards electrochemical miRNA detection using an affordable paper-based strategy. *Anal. Bioanal. Chem.* **2024**, *416*, 4227-4239.
27. Fu, Y.; Wang, N.; Yang, A.; Xu, Z.; Zhang, W.; Liu, H.; Law, H.K.; Ultrasensitive detection of ribonucleic acid biomarkers using portable sensing platforms based on organic electrochemical transistors. Anal. Chem. **2021**, *93*, 14359−14364.
28. Peng, J.; He, T.; Sun, Y.; Liu, Y.; Cao, Q.; Wang, Q.; Tang, H. A Route to the colorimetric detection of alpha-fetoprotein based on a smartphone. Micromachines **2024**, *15*, 1116.
29. Zhu, D.; Hu, Y.; Zhang, X.-J.; Yang, X.-T.; Tang, Y.-Y. Colorimetric and Fluorometric Dual-Channel Detection of α-Fetoprotein Based on the Use of ZnS-CdTe Hierarchical Porous Nanospheres. Microchim. Acta **2019**, *186*, 124.
30. Sun, C.; Pan, L.; Zhang, L.; Huang, J.; Yao, D.; Wang, C.-Z.; Zhang, Y.; Jiang, N.; Chen, L.; Yuan, C. A Biomimetic Fluorescent Nanosensor Based on Imprinted Polymers Modified with Carbon Dots for Sensitive Detection of Alpha-Fetoprotein in Clinical Samples. Analyst **2019**, *144*, 6760–6772.
31. Xie, B.; Wang, H.; Mochiwa, Z.O.; Zhou, D.; Gao, L. Highly sensitive detection of alpha-fetoprotein using sandwich sensors. *RSC Adv.* **2024**, *14*, 34661-34667.
32. Sun, Y.; Hou, Y.; Cao, T.; Luo, C.; Wei, Q. A Chemiluminescence Sensor for the Detection of α-Fetoprotein and Carcinoembryonic Antigen Based on Dual-Aptamer Functionalized Magnetic Silicon Composite. Anal. Chem. **2023**, *95*, 7387-7395.
33. Liu, J.; Jing, T.; Qi, H.; Zhao, Y.; Wu, M. A nano-silver modified heterojunction of bismuth sulfide nanoflowers–titania nanorods for sensitively detecting alpha-fetoprotein. New J. Chem. **2025**, *49*, 7918-7927.
34. Su, X.; Chem. J.; Wu, S.; Qiu, Y.; Pan, Y.. A Signal-On Microelectrode Electrochemical Aptamer Sensor Based on AuNPs–MXene for Alpha-Fetoprotein Determination. Sensors ***2024***, *24, 7878*.
35. Thakur, B.; Anbalagan, A.C.; Koyande, P.; Sawant, S.M. Electrochemical surface plasmon resonance based biosensor for α-fetoprotein detection via different coupling strategies. *Sci. Rep.* **2025**, *15*, 16902.
36. Ma, H.; Sun, X.; Chen, L.; Cheng, W.; Han, X.X.; Zhao, B.; He, C.. Multiplex Immunochips for High-Accuracy Detection of AFP-L3% Based on Surface-Enhanced Raman Scattering: Implications for Early Liver Cancer Diagnosis. Anal. Chem. **2017**, *89*, 8877-8883.

 doi:10.20944/preprints202509.1375.v1

37. Cong, B.; Liang, W.; Lai, W.; Jiang, M.; Ma, C.; Zhao, C.; Jiang, W.; Zhang, S.; Li, H.; Hong, C. A signal amplification electrochemiluminescence biosensor based on Ru (bpy)$_3^{2+}$ and β-cyclodextrin for detection of AFP. *Biochem.* **2024**, *156*, 108626.
38. Lim, J.Y.; Lee, S.S. A QCM immunosensor employing signal amplification strategies by enlarging the size of nanoparticles using gold or silver staining. Analyst **2022**, *147*, 5725-5731.
39. Stevens, R.J.; Poppe, K.K. Validation of clinical prediction models: what does the "calibration slope" really measure? J. Clin. Epidemiol. **2020**, *118*, 93-99.